Hybrid Coupling Between Long-Range Surface Plasmon Polariton Mode and Dielectric Waveguide Mode

Fang Liu, Yunxiang Li, Ruiyuan Wan, Yidong Huang, Xue Feng, and Wei Zhang

***Abstract*—In this paper, the hybrid coupling between long-range surface plasmon polariton (LRSPP) waveguide mode and dielectric waveguide mode has been studied theoretically and experimentally in detail by considering its dependence on the structure parameters and wavelength. It is demonstrated that extremely high coupling efficiency ($>99\%$) has been achieved for TM polarization, while no coupling could happen for TE polarization between these two kinds of waveguides. Based on this hybrid coupler, a polarization splitter with pure TM-mode output from one arm and TE-mode output from the other arm with high TE/TM extinction ratio has been realized. Additionally, this kind of coupling between different waveguides is very significant for providing an effective approach to connect the LRSPP-based devices with the conventional dielectric devices.**

***Index Terms*—Hybrid coupler, polarization splitter, surface plasmon polariton (SPP).**

I. Introduction

SURFACE plasmon polariton (SPP) is a kind of transverse magnetic (TM) surface electromagnetic excitation that propagates in a wave-like fashion along the interface between metal and dielectric medium [1], [2]. It has shown the unique characteristics and potential applications on integrated optical circuit, sensing, subwavelength lithography, and so on [3]–[12]. For a thin metal film embedded in dielectrics, the SPPs on the upper and lower metal–dielectric interfaces couple and form two modes, one is a symmetric mode and the other is an asymmetric mode. The symmetric mode with its field extending into the dielectrics has comparatively lower loss and is referred to as long-range SPP (LRSPP) [2], [13]. The metal strip guided LRSPP modes, so-called LRSPP waveguide modes, had been studied [14]–[16], and research on various LRSPP-based optical devices had been reported, such as splitter, modulator, sensor, and so on [17]–[20]. The SPP devices, especially the LRSPP devices, are considered as one of the important routes to realize integrated optical devices in the future.

Recently, we proposed the hybrid coupler, which consists of an LRSPP waveguide and dielectric waveguide(s), and predicted theoretically that high efficient coupling can occur between the LRSPP waveguide mode and the dielectric waveguide modes [21]–[23]. Compared with the pure LRSPP coupler [17], [18], the proposed hybrid coupler has not only the same advantages provided by the pure LRSPP coupler, but also lower loss and other functions, such as exciting LRSPP mode in integrated devices, realizing high-performance TE/TM-mode splitter, high-sensitive refractive index sensor, and variable optical attenuation [24]. Additionally, this kind of hybrid coupling is very significant for providing an effective approach to connect the SPP devices with dielectric devices and an integratable method to excite other SPP modes, such as short-range SPP (SRSPP) mode, which has drawn attention recently for its promising applications [25], [26].

Following our theoretical work, two research groups have fabricated the horizontal and vertical two-arm hybrid coupler, respectively, and observed the coupling phenomena between the LRSPP mode and dielectric waveguide mode [27], [28]. However, the coupling efficiency was not high enough until we demonstrated the hybrid coupler comprised of an Au strip and an SiN strip embedded in SiO_2. An extremely high efficient coupling ($>99\%$) between these two kinds of modes has been demonstrated successfully [29]. This paper is an extension of our earlier reported results [21], [29]. The coupling between LRSPP waveguide mode and dielectric waveguide mode has been discussed theoretically and experimentally in detail by considering its dependence on the structure parameters and wavelength.

This paper is organized as follows. Section II describes the structure of the hybrid coupler and the fabrication processes. In Section III, the simulation method and the measurement setup is described. In Section IV, the coupling characteristics of TE mode (see Section IV-A) and TM mode versus structure parameters (see Section IV-B) and wavelength (see Section IV-C) are analyzed theoretically and experimentally. Section V gives a conclusion of this paper.

II. Structure and Fabrication

The schematic structure of the hybrid coupler is illustrated in Fig. 1(a), in which the horizontal Au strip (yellow) and SiN strip (gray) are surrounded by SiO_2. The length of the hybrid

Manuscript received July 29, 2010; revised September 20, 2010, October 17, 2010, December 20, 2010, January 31, 2011; accepted February 08, 2011. Date of publication February 17, 2011; date of current version April 11, 2011. This work was supported in part by the National Basic Research Program of China (973 Program under Contracts 2011CB301803, 2010CB327405, and 2007CB307004), and in part by the National Natural Science Foundation of China under Grants NSFC-60537010 and NSFC-60877023.

The authors are with the State Key Laboratory of Integrated Optoelectronics, Department of Electronic Engineering, Tsinghua University, Beijing 100084, China (e-mail: liu_fang@tsinghua.edu.cn; liyx05@gmail.com; wry06@mails.tsinghua.edu.cn; yidonghuang@tsinghua.edu.cn; x-feng@tsinghua.edu.cn; zwei@tsinghua.edu.cn).

Color versions of one or more of the figures in this paper are available online at http://ieeexplore.ieee.org.

Digital Object Identifier 10.1109/JLT.2011.2115992

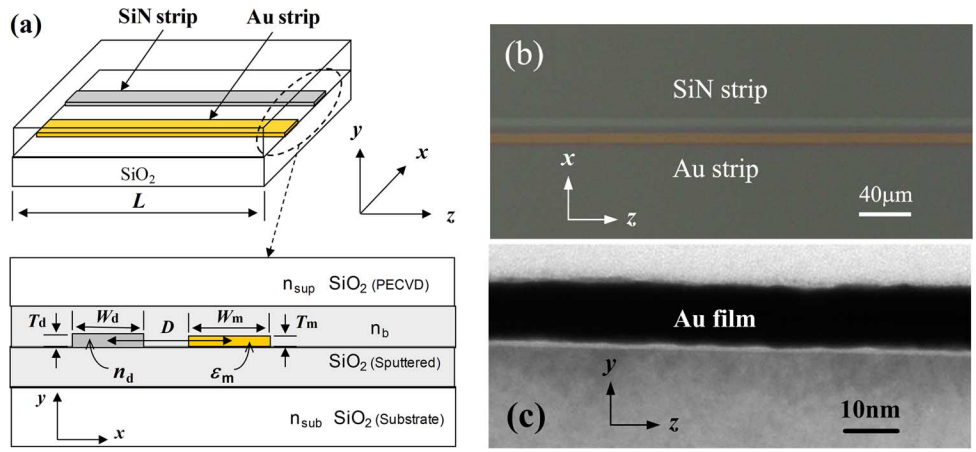

Fig. 1. (a) Schematic structure of the hybrid coupler with Au strip (yellow) and SiN strip (gray) surrounded by SiO_2. The cross section in the *xy* plane shows the definition of the structure parameters. (b) Top view of the hybrid coupler under microscope. (c) Photo of the Au film by transmission electron microscope.

coupler along propagation direction is L, and the cross section of the coupler with detailed structure parameters is also shown.

To fabricate the hybrid coupler, an Si wafer covered by a 15 μm thick SiO_2 layer (with refractive index $n_{\rm sub} = 1.446$) is selected as the substrate. A 9 μm thick SiO_2 layer ($n_{\rm sup} = 1.448$) is deposited by plasma-enhanced chemical-vapor deposition (PECVD) to cover the whole structure as the superstrate at the end of the processes. Since the LRSPP mode has small refractive index difference tolerance between the substrate and superstrate [14], [30], to reduce the refractive index difference between the SiO_2 substrate and the SiO_2 prepared by PECVD, two 1 μm thick SiO_2 buffer layers are sputtered, respectively, above and beneath the Au film with almost the same refractive index ($n_{\rm b} = 1.453$) to make sure that LRSPP mode can be supported by the Au strip.

Between the two 1 μm thick sputtered SiO_2 buffer layer, the horizontal Au and SiN strip are fabricated as follows. A SiN ($n_{\rm d} = 1.871$) layer with thickness $T_{\rm d}$ is prepared by PECVD on the 1 μm thick SiO_2 buffer layer. Then by adopting standard UV lithography, photoresist strip pattern is formed on the SiN layer with different width $W_{\rm d}$. After dry etching process by reactive ion etching and removing the photoresist, the SiN waveguides with different width $W_{\rm d}$ on SiO_2 layer are fabricated. Next, the $W_{\rm m} = 8$ μm wide and $T_{\rm m} = 12$ nm thick Au strips are fabricated by cover lithography, magnetic sputtering of Au, and lift-off process with the help of the photoresist remover. For the process of cover lithography, which is to fabricate the concave photoresist strip by adopting the UV lithography again, it is very important to make sure that the Au strip (concave photoresist strip) is parallel to the SiN waveguide, and meanwhile the distance D between these two different arms is 11 μm.

Fig. 1(b) shows the top view of the hybrid coupler under microscope. To fabricate the LRSPP waveguide with required thickness, the Au sputtering speed is controlled as 2–3 nm/min. The Au film with thickness of 10 nm level is observed by the transmission electron microscope and the photo is shown in Fig. 1(c).

In this paper, as described earlier, the parameters of LRSPP waveguide (Au strip) and the distance D between the two kinds of waveguides is fixed, and we adjusted the width $W_{\rm d}$ and thickness $T_{\rm d}$ of SiN waveguide to analyze the coupling characteristics theoretically and experimentally. Here, the name of the hybrid coupler is defined as HC $(T_{\rm d}, W_{\rm d})$ according to the parameters of the SiN waveguide. The theoretical analysis carried out on the hybrid coupler in Section IV is based on the actual fabricated structure with parameters described earlier. In our model, the metal strip is wide enough and can be considered as a metal film when considering the metal–dielectric constant. So, the complex dielectric constant of the Au film $\varepsilon_{\rm m}$ in [31] is adopted for simulation. In the next section, the simulation and measurement method will be described.

III. Simulation and Measurement Method

A. Simulation Method

To analyze the coupling between the LRSPP and dielectric waveguide mode, the coupled eigenmodes, including the electromagnetic fields in xy plane and propagation constants, are calculated directly with the help of the software COMSOL [32], which implements the finite element method to solve Maxwell's equations and have been adopted by lots of researchers to calculate the SPP waveguide eigenmode rigorously [32]–[34].

It is known that any mode supported by the hybrid coupler can be expressed in terms of a linear superposition of the eigenmodes supported by the coupler [21], [22], [35]

$$\boldsymbol{H}(x,y,z) = \sum_j a_j \boldsymbol{H}_j(x,y) e^{i\beta_j z} \tag{1a}$$

$$\boldsymbol{E}(x,y,z) = \sum_j a_j \boldsymbol{E}_j(x,y) e^{i\beta_j z} \tag{1b}$$

where the subscript j is the index number of the eigenmode, $\boldsymbol{H}_{\rm j}$ and $\boldsymbol{E}_{\rm j}$ are the magnetic fields and electronic fields of the eigenmodes when $z = 0$, and $\beta_{\rm j}$ and $a_{\rm j}$ are the corresponding complex propagation constant and modes constant, respectively. Here, the field imaginary part of the LRSPP mode is much smaller than the real one. So, we just consider the real part of the field when studying the coupling characteristics, which is different from the high-loss SRSPP mode [25].

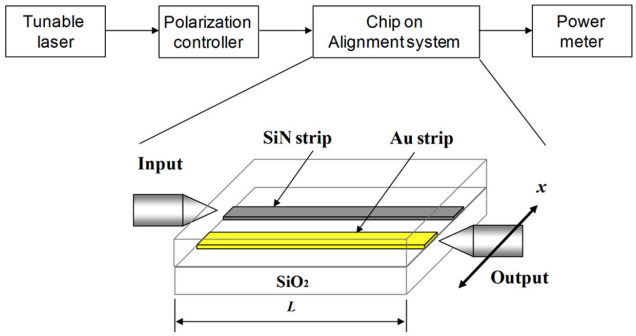

Fig. 2. Setup of the measurement system composed of a tunable laser, a polarization controller, a precise fiber alignment system, two tapered lens fibers, and a power meter.

We consider launching the mode of the individual dielectric waveguide $\boldsymbol{H}_{\mathrm{SiN}}$ ($\boldsymbol{E}_{\mathrm{SiN}}$) as the input, and the amplitudes of the even and odd eigenmodes can be derived from [36]

$$a_j = \frac{1}{2}\int (\boldsymbol{E}_{\boldsymbol{S}iN} \times \boldsymbol{H}_j{}^*)\cdot \widehat{z}\ \, dx\, dy \tag{2}$$

where all the modes have been normalized

$$\frac{1}{2}\int (\boldsymbol{E}_j \times \boldsymbol{H}_j{}^*)\cdot \widehat{z}\ \, dx\, dy = 1. \tag{3}$$

The analysis of Section IV would show that there is just one eigenmode for TE mode, and there exist two eigenmodes for TM mode. The coupling length of the TM mode is defined as

$$L_{\mathrm{c}} = \pi/(|\beta_{\mathrm{er}} - \beta_{\mathrm{or}}|) \tag{4}$$

here, β_{er} and β_{or} are the real part of the propagation constant of the two coupled TM eigenmodes.

Thus, with the calculated eigenmodes (fields and propagation constants) and (1)–(4), the coupling characteristics between the LRSPP mode and dielectric waveguide mode can be studied theoretically.

B. Measurement Method

The setup of the measurement system for studying the coupling characteristics of the hybrid coupler is shown in Fig. 2. It includes a tunable laser (1350–1630 nm), a polarization controller, an input tapered lens fiber, a precise fiber alignment system, an output tapered lens fiber, and a power meter. The polarization controller is adopted to control the polarization (TM and TE) of the input light to investigate the coupling characteristics for different polarization. Tapered lens fibers are used to decrease the influence of noises at the input and output end.

To measure the output power distribution, we fix the input fiber to the center of the SiN waveguide at the input end and scan the output fiber with mode size of 1 μm along x axis at the other end. We also fix the input and output fibers, and vary the wavelength of the laser to study the wavelength dependence of the coupler. The tunable laser, precise fiber alignment system, and the power meter can be controlled by a computer through GPIB card for scanning the output power distribution and the wavelength automatically.

IV. Simulation and Measurement Results

For the Au strip with the parameters described in Section II, no higher order LRSPP mode [14] can be supported. The SiN waveguide with selected parameters can also only guide fundamental mode, whose real part of mode propagation constant is much smaller than that of the SRSPP mode [25]. Therefore, we only consider the coupling between the fundamental LRSPP mode and the dielectric waveguide mode.

In Section IV-A, the coupling characteristics of TE mode between two kinds of waveguides are discussed. In Section IV-B, we fix the wavelength at 1.55 μm to discuss how structure parameters of SiN waveguide affect the coupling of TM mode. In Section IV-C, the wavelength dependence of the TM-mode coupling is analyzed. Section IV-D gives a brief conclusion of the coupling characteristics.

A. No Coupling Happens for TE Mode

For the reason that LRSPP mode is TM polarized [13]–[15], no coupling happens between the TE-polarized dielectric waveguide mode and the LRSPP mode. Therefore, no matter how we adjust the width and thickness of SiN waveguide and the wavelength of the input light, the hybrid coupler can only support the TE eigenmode as shown in Fig. 3(a) (there is no higher order TE mode of dielectric waveguide). The mode field is similar to that just guided by the left dielectric arm and there is little field surrounding the right LRSPP arm. Accordingly, only one mode should be considered from (1)–(3). When the TE-polarized input is applied on the SiN waveguide, a 2-D field intensity profile in xy plane can be derived for a certain z. And for easy depiction of the energy coupling along z-direction, the 2-D profile is converted to the 1-D curve after the integral along y-axis, which is shown in Fig. 3(b). It can be seen that the energy propagates directly through the SiN waveguide without any coupling between these two waveguides.

The fabricated samples with different length L are measured, and the results are consistent with the theoretical prediction shown in Fig. 3(b). Taking the sample HC(32 nm, 6 μm) with $L = 1.7$ mm, for example, Fig. 4 shows the measured output intensity distribution of four samples with different marks and the simulated 2-D TE output power profile corresponding to Fig. 3(b). It can be seen that the measured results are well fitted by the blue solid line of the simulation result, which is the optical power received by the tapered fiber with 1 μm mode size along the white-dashed line marked in the inset. Varying the input wavelength, similar measurement results are obtained that no TE output can be detected from the Au strip.

B. Coupling Characteristics of TM Mode Versus Structure Parameters

For TM polarization, the individual Au strip (without SiN strip) can support the LRSPP waveguide mode with propagation constant $\beta_{\mathrm{LRSPP}} = \beta_{\mathrm{LRSPPr}} + i \times \beta_{\mathrm{LRSPPi}}$, and the individual SiN strip (without Au strip) can support the fundamental dielectric waveguide mode with propagation constant β_{SiN}. According to the coupled mode theory [36], when combining the Au strip with SiN strip together as shown in Fig. 1, we could get two TM coupled eigenmodes, even ($\beta_{\mathrm{e}} = \beta_{\mathrm{er}} + i \times \beta_{\mathrm{ei}}$) and odd mode ($\beta_{\mathrm{o}} = \beta_{\mathrm{or}} + i \times \beta_{\mathrm{oi}}$). Their propagation constants

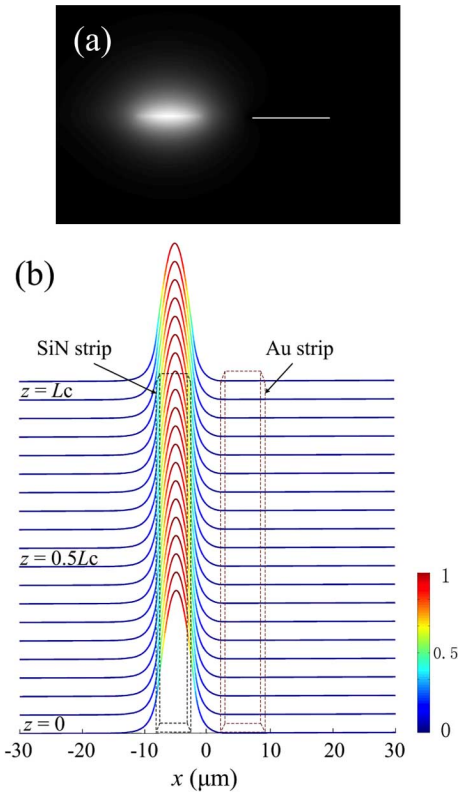

Fig. 3. (a) Amplitude of magnetic field $|H_{\mathrm{TE}}|$ of the TE eigenmode in xy plane. (b) TE mode power propagates directly through the SiN waveguide. Here, $W_{\mathrm{d}} = 6\ \mu$m, $T_{\mathrm{d}} = 32$ nm, and $\lambda_0 = 1.55\ \mu$m.

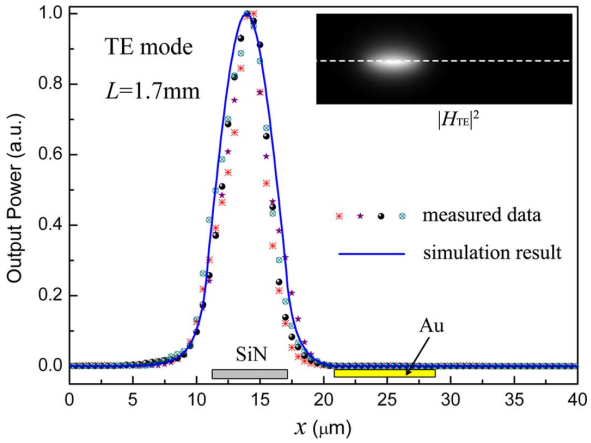

Fig. 4. TE mode output power profile along x axis measured from four samples when input is applied on the SiN waveguide. The inset is the simulated 2-D TE output energy profile in the xy plane. The blue solid line is the optical power received by the tapered fiber with 1 μm mode size along the white-dashed line in the inset. Here, $W_{\mathrm{d}} = 6\ \mu$m, $T_{\mathrm{d}} = 32$ nm, and $\lambda_0 = 1.55\ \mu$m.

(β/k_0) at $\lambda_0 = 1.55\ \mu$m are shown in Fig. 5 for the fixed thickness $T_{\mathrm{d}} = 32$ nm and varied width of the SiN waveguide W_{d}.

Fig. 5(a) shows that the β_{SiN} is close to β_{LRSPPr} (close to the cross point of the two solid lines) when $W_{\mathrm{d}} = 6\,\mu$m, and the two coupled eigenmodes of HC(32 nm, 6 μm) have the symmetric filed profile as shown in Fig. 6(a). For the even mode, the magnetic field has the same direction in all the position with more concentrated field near the waveguide. While the odd mode has opposite field direction on the two arms and has a dip ($|\boldsymbol{H}| = 0$)

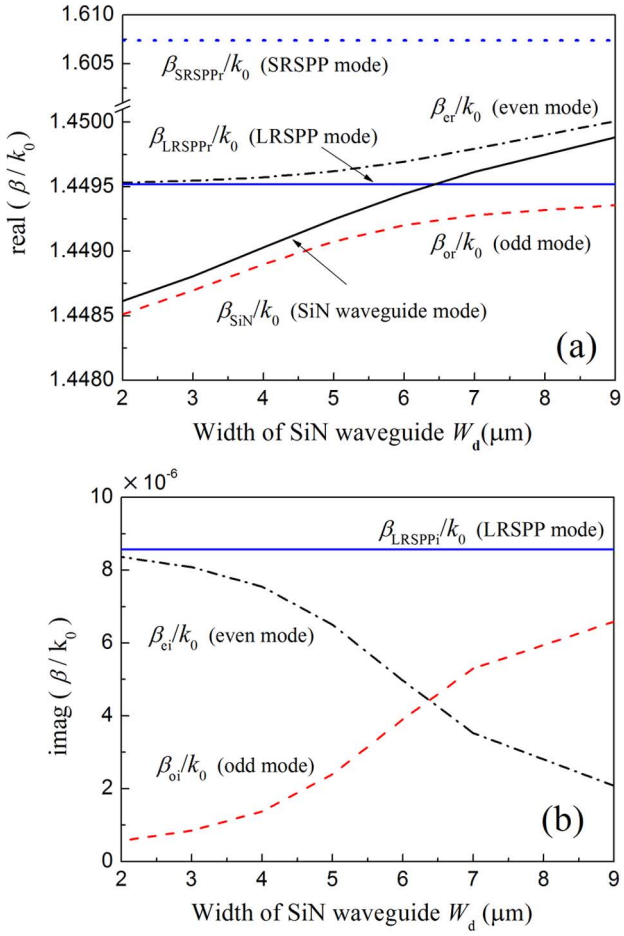

Fig. 5. (a) Real part of propagation constant of the modes before and after coupling when varying the width of SiN waveguide W_{d} [37]. (b) Imaginary part of the propagation constant of the mode as a function of W_{d}. Here, $T_{\mathrm{d}} = 32$ nm and $\lambda_0 = 1.55\ \mu$m.

at the center of the coupler. The high field symmetry also results in the close β_{ei} and β_{oi} (close propagation loss) as shown in Fig. 5(b).

Therefore, using the mode field and propagation constant of the coupled eigenmodes, the energy coupling between the two waveguides along z-direction can be derived and shown in Fig. 6(b) when input is applied on the SiN waveguide at $\lambda_0 = 1.55\ \mu$m according to (1)–(3). When $z = 0$, the mode profile is identical to the input mode guided by dielectric waveguide and with no energy guided by Au strip. When $z = L_{\mathrm{c}}/2$, the energy has symmetric profile with almost equal energy on both arms. When $z = L_{\mathrm{c}}$, almost all of the energy is guided by the Au strip, and the dielectric waveguide mode transforms to LRSPP mode completely. Therefore, the high symmetry of the eigenmodes shown in Fig. 6(a) means high efficient coupling between the LRSPP and dielectric waveguide mode.

For HC(32 nm, 6 μm), the measurement results of the normalized output power coupled to the Au waveguide (red square) and remained in the SiN waveguide (purple dot) with different interaction length L from 0.5 to 2.6 mm are shown in Fig. 7. The measurement result indicates that the input energy transfers gradually from the SiN waveguide to the LRSPP waveguide, which proves the theoretical results shown in Fig. 6(b). The

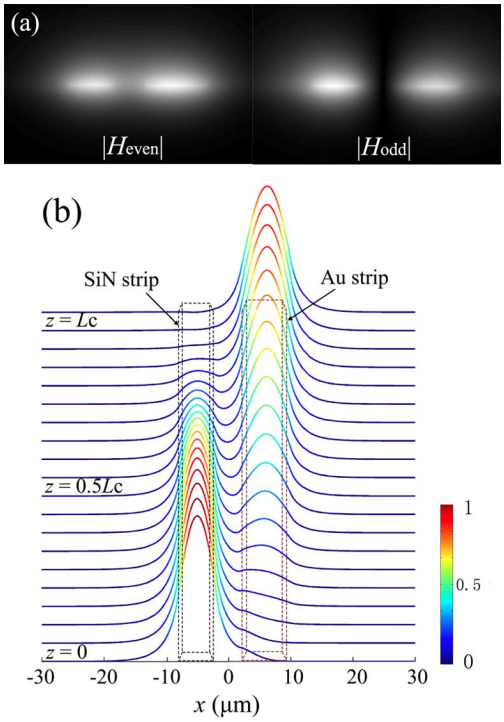

Fig. 6. For HC(32 nm, 6 μm) at $\lambda_0 = 1.55$ μm. (a) Amplitude of magnetic field $|H|$ of the two TM eigenmodes in xy plane. (b) Power of TM-polarized energy couples from SiN strip to Au strip along propagation direction z. Here, $W_d = 6$ μm, $T_d = 32$ nm, and $\lambda_0 = 1.55$ μm.

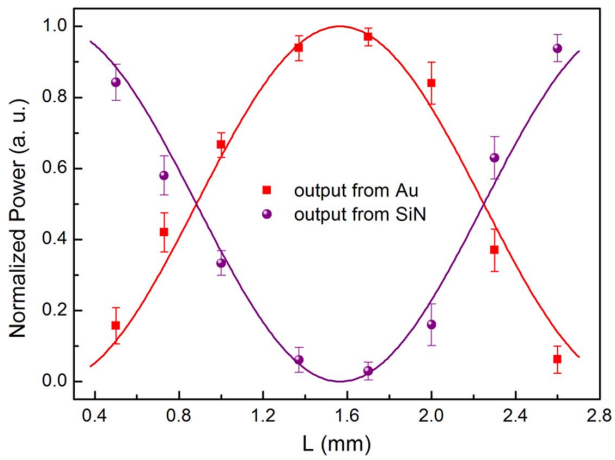

Fig. 7. Normalized output power from Au strip (square) and SiN strip (dot) with various interaction lengths when input is applied on the SiN waveguide. The measured data are well fitted by the solid curves of $\sin^2$. Here, $W_d = 6$ μm, $T_d = 32$ nm, and $\lambda_0 = 1.55$ μm.

measured power versus L at the output end of both waveguides are well fitted by the solid curves of $\sin^2(|\beta_{er} - \beta_{or}| \times L/2)$.

Fig. 8(a) and (b) shows the output power distribution along x axis measured for the samples of $L = 0.7$ and 1.7 mm, respectively. The simulated 2-D output power profile, which corresponds to Fig. 6(b) at different reaction length, are also shown as the inset of Fig. 8. The measured data are well fitted by the solid line, which is the simulated optical power received by the tapered fiber along the white-dashed line marked in the corresponding inset. It is can be seen that, for the case of $L = 0.7$ mm,

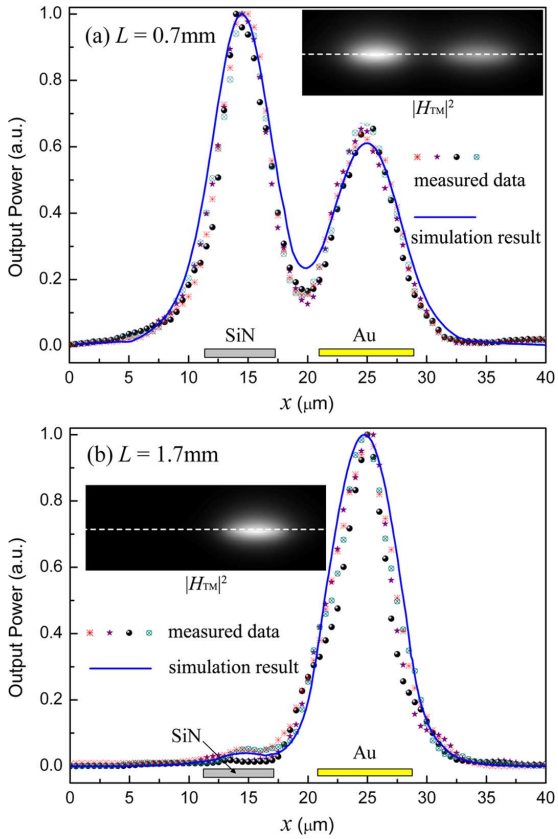

Fig. 8. TM-mode output power profile of four samples along x axis with reaction length (a) $L = 0.7$ mm, (b) $L = 1.7$ mm, where the input is applied on the SiN waveguide. The inset is the corresponding simulated 2-D TM output power profile in the xy plane. The blue solid line is the optical power received by the tapered fiber with 1 μm mode size along the white-dashed line in the inset. Here, $W_d = 6$ μm, $T_d = 32$ nm, and $\lambda_0 = 1.55$ μm.

almost 40% of the energy couples from SiN waveguide to Au (LRSPP) waveguide, while when $L = 1.7$ mm, 98% of the energy couples to the Au waveguide with little energy remaining in the input SiN waveguide.

For HC(32 nm, 5 μm), the $|\beta_{LRSPPr} - \beta_{SiN}|$ is larger than that of HC(32 nm, 6 μm), as shown in Fig. 5. The even and odd modes illustrate the obvious unsymmetric filed profile shown by Fig. 9(a). The even mode has more energy on the Au waveguide side and the odd mode has more energy on the SiN waveguide side, which results in the incomplete coupling between these two waveguides. The samples of HC(32 nm, 5 μm) with different length are also measured, and the normalized output power from the two waveguides are shown in Fig. 9(b), which illustrates that the maximum coupling efficiency is only about 85%. Fig. 9(c) shows the output power distribution along x axis when $L = 1.7$ mm with part of the energy remaining in the input SiN waveguide. Similarly, the simulation results are given in Fig. 9 and well fitted to the measured data.

Furthermore, the coupling characteristics of the hybrid coupler with different parameters of the SiN waveguide are measured in detail, and the results are shown in Table I. It is illustrated that HC(32 nm, 6.5 μm) can also achieve a high coupling efficiency to 98% similar to HC(32 nm, 6 μm), which results from the rather close β_{SiN} and β_{LRSPPr} as shown in Fig. 5(a). While the coupling efficiency of HC(43 nm, 5 μm) and HC(43

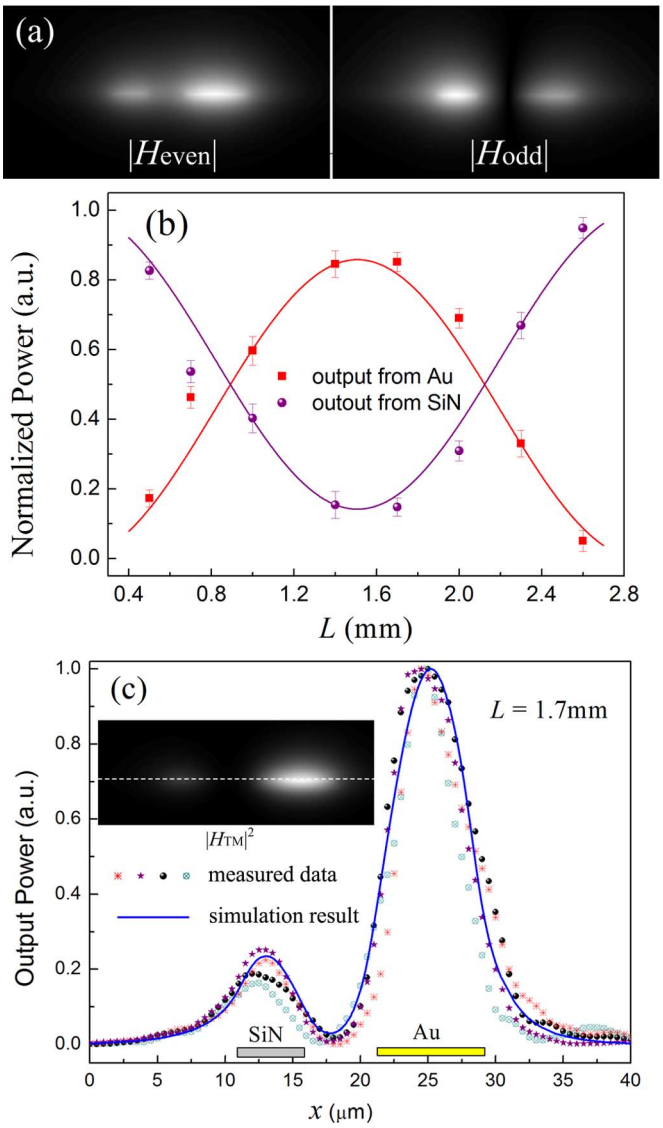

Fig. 9. For HC(32 nm, 5 μm) at $\lambda_0 = 1.55$ μm. (a) Amplitude of magnetic field $|\boldsymbol{H}|$ of the two TM eigenmodes in xy plane. (b) Normalized output power from Au strip (square) and SiN strip (dot) with various interaction lengths when input is applied on the SiN waveguide. (c) TM mode output power profile when $L = 1.7$ mm with corresponding simulation results in the inset. The blue solid line is the optical power received by the tapered fiber with 1 μm mode size along the white-dashed line in the inset.

TABLE I
COUPLING CHARACTERISTICS VERSUS STRUCTURE PARAMETER

(T_d, W_d)	L**	Coupling efficiency @ L	Loss
(32nm, 5μm)	~1.7mm	85%@1.7mm	1.19dB/mm
(32nm, 6μm)	~1.7mm	98%@1.7mm	1.5379/mm
(32nm, 6.5μm)	~2.0mm	98%@2.0mm	1.03dB/mm
(43nm, 5μm)	~1.5mm	70%@1.5mm	0.54dB/mm
(43nm, 6μm)	~1.3mm	27%@1.3mm	0.44dB/mm

* λ_0 is fixed as 1.55μm, the size of Au strip is fixed as W_m=8μm, T_m = 12nm, and the waveguides distance is fixed as D=11μm.
** The sample length corresponding to the highest coupling efficiency.

nm, 6 μm) is not very high, which results from the mismatch between β_{SiN} and β_{LRSPPr}.

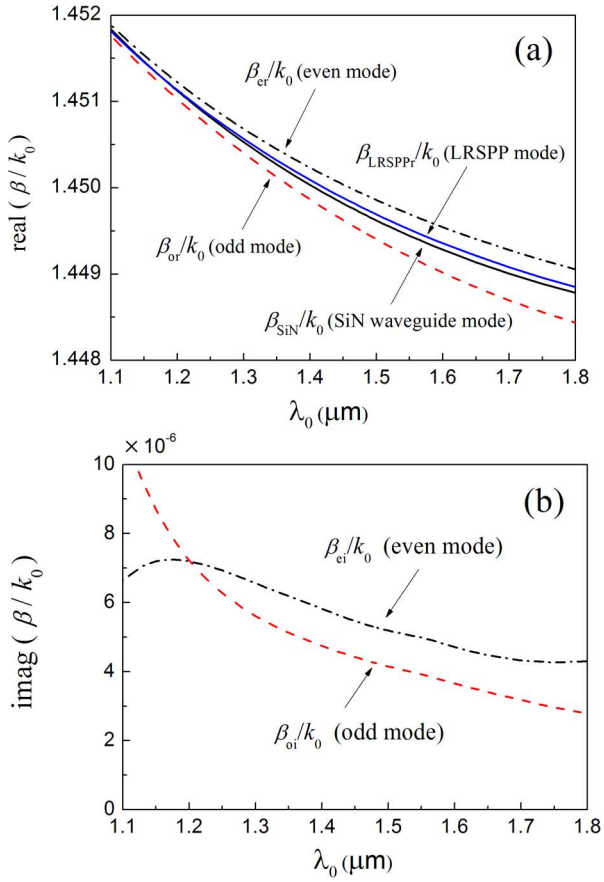

Fig. 10. For HC(32 nm, 6 μm). (a) Real part of propagation constant of the modes before and after coupling as a function of wavelength λ_0 and the coupling length in the inset. (b) Imaginary part of propagation constant of the two coupled eigenmodes.

Meanwhile, the loss of the hybrid coupler is also shown in Table I. Even though the loss along propagation direction is not uniform (higher loss when more energy guided by Au strip, lower loss when more energy guided by SiN strip), the average loss per unit length is estimated. The results indicate that smaller loss corresponds to the lower coupling efficiency, which can be understood by considering that less proportion of the energy is guided by the lossy metal strip of the hybrid coupler.

C. Coupling Characteristics of TM Mode Versus Wavelength

In this section, the wavelength dependence of the TM-mode coupling is analyzed for HC(32 nm, 6 μm) and HC(32 nm, 5 μm).

For HC(32 nm, 6 μm), Fig. 10 illustrates the (a) real part and (b) imaginary part of the propagation constant of the two coupled eigenmodes, as well as the individual waveguide modes, as a function of wavelength. Since the β_{LRSPPr} of individual LRSPP waveguide mode is close to the β_{SiN} of individual SiN waveguide mode, the field profile of the even and odd mode has a symmetric profile at different wavelength similar to those shown in Fig. 6(a).

Since the coupling efficiency of the two individual modes is mainly decided by the match of their propagation constant [36] and indicated by the symmetry of the eigenmodes as discussed in Section IV-B, the two close solid lines in Fig. 10(a) mean high

coupling efficiency can be obtained at different wavelength with the corresponding coupling length. The analysis and results of the coupling characteristics at a certain wavelength are similar to that in Section IV-B. Here, to be consistent with the actual situation, the wavelength dependence is studied with fixed device length L.

Fig. 11 illustrates the measurement results of the TM power coupled to the Au strip (square) and that remained in SiN waveguide (dot), which are fit by the simulation results (solid lines), as a function of the wavelength λ_0 from 1.350 to 1.625 μm when (a) $L = 1.4$ mm, (b) $L = 1.7$ mm, and (c) $L = 2.3$ mm.

As shown in Fig. 11(b), the coupling efficiency is rather high ($>99\%$) in the wavelength range from 1.465 to 1.510 μm and an extremely high coupling efficiency, as high as 99.75%, is observed at $\lambda_0 = 1.485$ μm. That is because $L = 1.7$ mm is very close to the coupling length L_c at $\lambda_0 = 1.485$ μm. When $\lambda_0 = 1.55$ μm, the energy remaining in the SiN waveguide is about 2%, which corresponds to the measurement results of output power distribution shown in Fig. 8(b).

However, the coupling efficiency shown in Fig. 11(a) cannot be as high as that shown in Fig. 11(b). The reason is that $L = 1.4$ mm equals to the coupling length at a certain wavelength λ^* ($\lambda^* > 1.625$ μm), which is not in the wavelength range of the tunable laser. Since the longer wavelength is closer to λ^*, Fig. 11(a) shows that the coupling efficiency increases as the wavelength λ_0 increases. Similarly, $L = 2.3$ mm corresponds to the wavelength λ^{**} ($\lambda^{**} < 1.35$ μm), and the coupling efficiency decreases as the wavelength λ_0 increases.

For HC(32 nm, 5 μm), the propagation constant of the two coupled eigenmodes is shown in Fig. 12(a) and (b). Compared with that shown in Fig. 10, β_{LRSPPr} and β_{SiN} of the two individual waveguide modes have much larger difference, and the filed profile of the coupled eigenmodes at different wavelength is similar to that shown in Fig. 9(a) with asymmetric distribution.

Fig. 12(c) shows the proportion of the output power from the Au and SiN waveguide when $L = 1.7$ mm. Although 1.7 mm is close to the coupling length of HC(32 nm, 5 μm) at $\lambda_0 = 1.550$ μm, as shown in Fig. 9(b), the result of Fig. 12(c) illustrates that the coupling efficiency varies monotonically with λ_0, which is different from that of Fig. 11(b). That is because the mode size affects the coupling more significantly than the coupling length for the 1.7 mm long HC(32 nm, 5 μm). The larger mode size at longer wavelength results in stronger coupling, which is illustrated by larger $|\beta_{\mathrm{er}} - \beta_{\mathrm{or}}|$ and smaller $|\beta_{\mathrm{ei}} - \beta_{\mathrm{oi}}|$, and less energy remaining in the SiN strip.

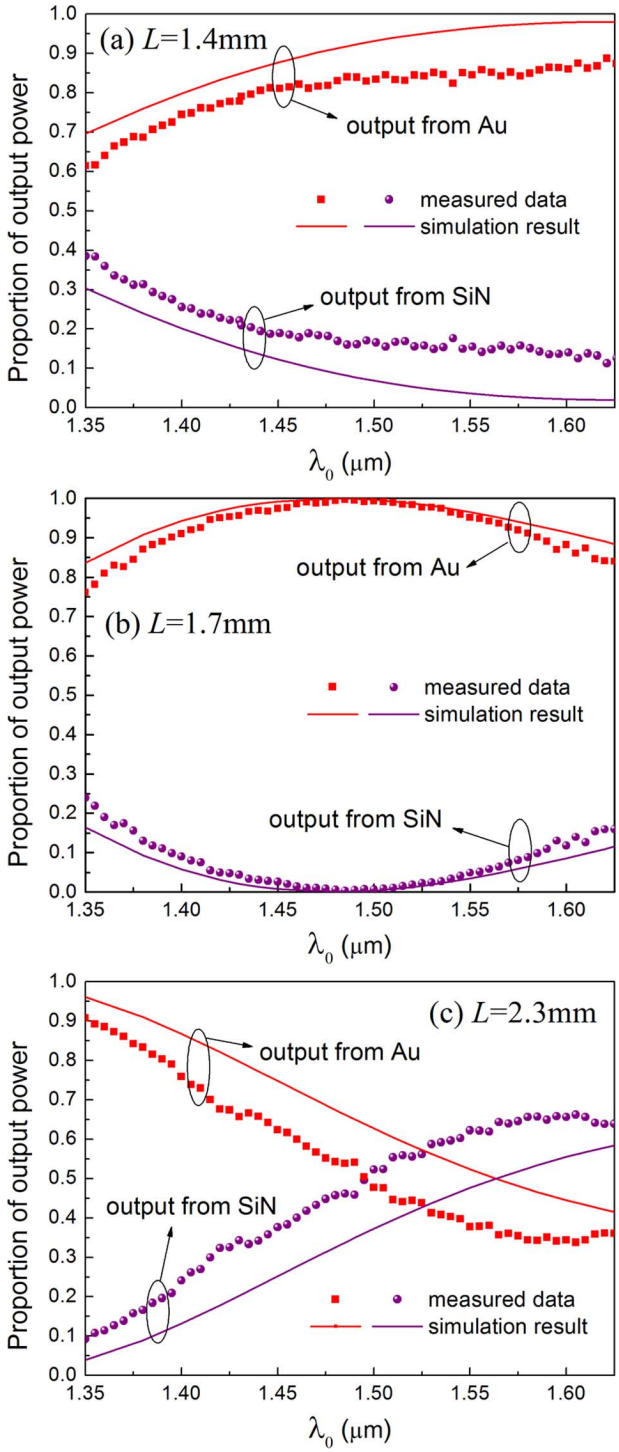

Fig. 11. Proportion of the TM power coupled to Au strip (square) and that remained in SiN waveguide (dot) as a function of wavelength when (a) $L = 1.4$ mm, (b) $L = 1.7$ mm, and (c) $L = 2.3$ mm. The solid line is the simulation results. Here, $W_d = 6$ μm and $T_d = 32$ nm.

D. Discussions

From the previous simulation and experimental results described in Sections IV-A–C, it can be seen that there is no coupling between the LRSPP and TE-polarized dielectric waveguide mode, and the coupling between the LRSPP and TM-polarized dielectric waveguide mode complies with the basic rules of the coupled mode theory. Although SPP is a kind of surface wave on the metal, the LRSPP mode looks much like a weak guided, lossy dielectric waveguide mode with most of the field extending into the surrounding dielectrics and comparative low propagation loss. The match of the propagation constant between the individual LRSPP and TM-polarized dielectric waveguide mode, which results in high-symmetric field distribution and close loss of the coupled eigenmodes, is still the most important factor for getting high coupling efficiency.

The simulation and measurement results have shown that the coupling characteristics are quite different between TE-

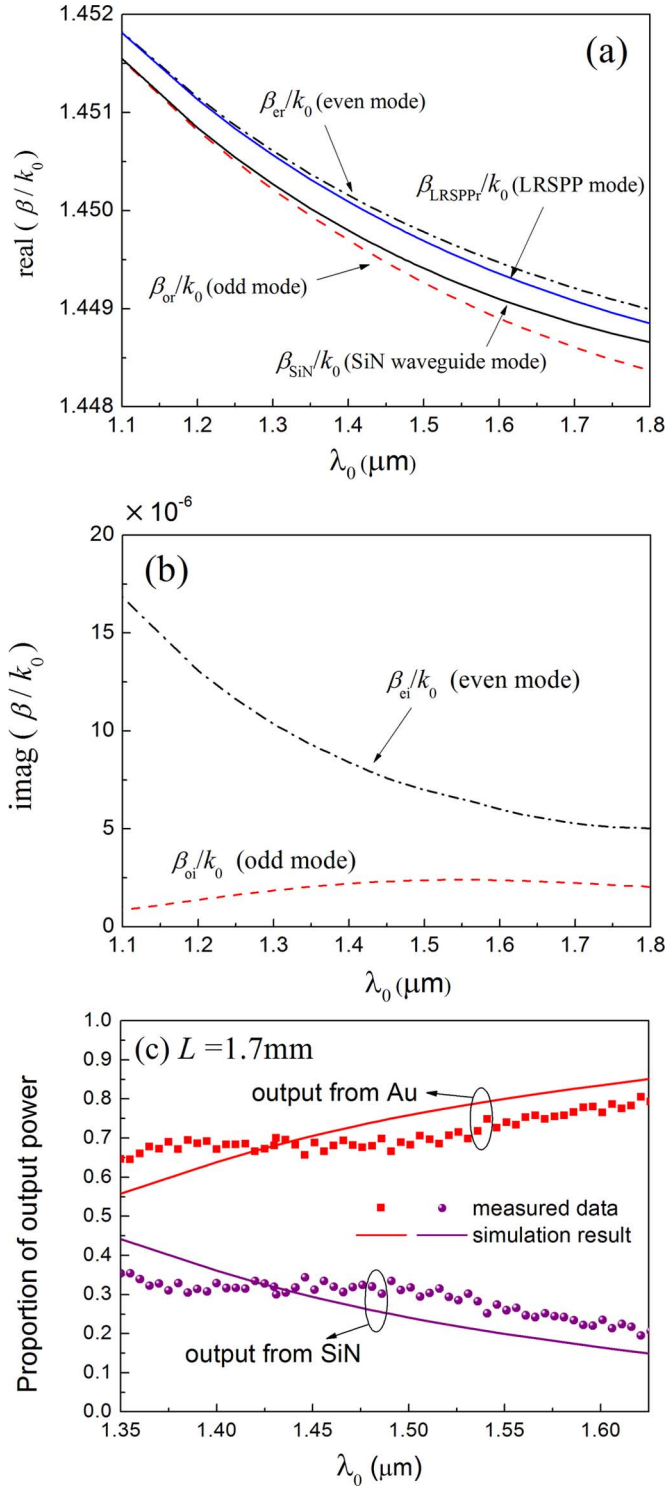

Fig. 12. For HC(32 nm, 5 μm). (a) Real part of propagation constant of the modes before and after coupling as a function of wavelength λ_0. (b) Imaginary part of propagation constant of the two coupled eigenmodes. (c) Proportion of the TM power coupled to Au strip (square) and that remained in SiN waveguide (dot) as a function of wavelength when $L = 1.7$ mm.

and TM-polarized modes. Therefore, a high-performance polarization splitter can be realized when input is applied on the dielectric (SiN) waveguide. Pure TM-mode output without any noise of TE mode can always be obtained from LRSPP waveguide (Au strip), no matter how the size of the waveguides and the wavelength are adjusted. The TE mode with high TE/TM extinction ratio output from the SiN waveguide can also be derived by choosing proper structure parameters.

V. Conclusion

In conclusion, coupling between the LRSPP and conventional dielectric waveguide mode has been studied theoretically and experimentally in detail by considering structure parameters and wavelength. It is shown that there is no coupling between the LRSPP and TE-polarized dielectric waveguide mode. And the match of the propagation constant of the LRSPP and TM-polarized dielectric waveguide mode is the key for getting high efficient coupling, which complies with the basic rules of the coupled mode theory.

Based on the hybrid coupler comprised of a horizontal Au and a SiN strip, an extremely high coupling efficiency $(>99\%)$ has been achieved for TM polarization, while no coupling could happen for TE polarization between these two kinds of waveguides. Therefore, this structure can be used to excite LRSPP mode efficiently with dielectric waveguide or realize a kind of compact, high performance, and electrical-controlled TE/TM-mode splitter or combiner. More importantly, this kind of coupling between different waveguides is very significant for providing an effective approach to connect the SPP-based devices with the conventional dielectric devices.

Acknowledgment

The authors would like to thank Prof. J. Peng of Tsinghua University, and D. Ohnishi and Y. Miura of ROHM Corporation for their valuable discussions and helpful comments.

References

[1] H. Raether, *Surface Plasmons*. Berlin, Germany: Springer-Verlag, 1988.
[2] A. V. Zayats, I. I. Smolyaninov, and A. A. Maradudin, "Nano-optics of surface plasmon polaritons," *Phys. Rep.*, vol. 408, pp. 131–314, 2005.
[3] W. L. Barnes, A. Dereux, and T. W. Ebbesen, "Surface plasmon subwavelength optics," *Nature*, vol. 424, pp. 824–830, 2003.
[4] E. Ozbay, "Plasmonics: Merging photonics and electronics at nanoscale dimensions," *Science*, vol. 311, pp. 189–193, 2006.
[5] S. I. Bozhevolnyi, V. S. Volkov, E. Devaux, J. Y. Laluet, and T. W. Ebbesen, "Channel plasmon subwavelength waveguide components including interferometers and ring resonators," *Nature*, vol. 440, pp. 508–511, 2006.
[6] X. Guo, M. Qiu, J. Bao, B. J. Wiley, Q. Yang, X. Zhang, Y. Ma, H. Yu, and L. Tong, "Direct coupling of plasmonic and photonic nanowires for hybrid nanophotonic components and circuits," *Nano. Lett.*, vol. 9, pp. 4515–4519, 2009.
[7] Z. Li, F. Hao, Y. Huang, Y. Fang, P. Nordlander, and H. Xu, "Directional light emission from propagating surface plasmons of silver nanowires," *Nano. Lett.*, vol. 9, pp. 4383–4386, 2009.
[8] Y. Fang, Z. Li, Y. Huang, S. Zhang, P. Nordlander, N. J. Halas, and H. Xu, "Branched silver nanowires as controllable plasmon routers," *Nano. Lett.*, vol. 10, pp. 1950–1954, 2010.
[9] X. D. Hoa, A. G. Kirk, and M. Tabrizian, "Towards integrated and sensitive surface plasmon resonance biosensors: A review of recent progress," *Biosens. Bioelectron.*, vol. 23, pp. 151–160 , 2007.
[10] P. Berini, "Bulk and surface sensitivities of surface plasmon waveguides," *New J. Phys.*, vol. 10, pp. 105010-1–105010-37, 2008.
[11] N. Fang, H. Lee, C. Sun, and X. Zhang, "Sub-diffraction-limited optical imaging with a silver superlens," *Science*, vol. 308, pp. 534–537, 2005.
[12] X. Luo and T. Ishihara, "Surface plasmon resonant interference nanolithography technique," *Appl. Phys. Lett.*, vol. 84, pp. 4780–4782 , 2004.
[13] P. Berini, "Long-range surface plasmon polaritons," *Adv. Opt. Photon*, vol. 1, pp. 484–588, 2009.

[14] P. Berini, "Plasmon-polariton waves guided by thin lossy metal films of finite width: Bound modes of symmetric structures," *Phys. Rev. B*, vol. 61, pp. 10484–10503, 2000.
[15] R. Charbonneau, P. Berini, E. Berolo, and E. Lisicka, "Experimental observation of plasmon-polariton waves supported by a thin metal film of finite width," *Opt. Lett.*, vol. 25, pp. 844–846, 2000.
[16] T. Nikolajsen, K. Leosson, I. Salakhutdinov, and S. I. Bozhevolnyi, "Polymer-based surface-plasmon-polariton stripe waveguides at telecommunication wavelengths," *Appl. Phys. Lett.*, vol. 82, pp. 668–670, 2003.
[17] R. Charbonneau, C. Scales, I. Breukelaar, S. Fafard, N. Lahoud, G. Mattiussi, and P. Berini, "Passive integrated optics elements based on long-range surface plasmon polaritons," *J. Lightw. Technol.*, vol. 24, no. 1, pp. 477–494, Jan. 2006.
[18] A. Boltasseva, T. Nikolajsen, K. Leosson, K. Kjaer, M. S. Larsen, and S. I. Bozhevolnyi, "Integrated optical components utilizing long-range surface plasmon polaritons," *J. Lightw. Technol.*, vol. 23, no. 1, pp. 413–422, Jan. 2005.
[19] T. Nikolajsen, K. Leosson, and S. I. Bozhevolnyi, "Surface plasmon polariton based modulators and switches operating at telecom wavelengths," *Appl. Phys. Lett.*, vol. 85, pp. 5833–5835, 2004.
[20] R. Slavík and J. Homola, "Ultrahigh resolution long range surface plasmon-based sensor," *Sens. Actuators B*, vol. 123, pp. 10–12, 2006.
[21] F. Liu, Y. Rao, Y. Huang, W. Zhang, and J. Peng, "Coupling between long range surface plasmon polariton mode and dielectric waveguide mode," *Appl. Phys. Lett.*, vol. 90, pp. 141101-1–141101-3, 2007.
[22] F. Liu, Y. Rao, X. Tang, R. Wan, Y. Huang, W. Zhang, and J. Peng, "Hybrid three-arm coupler with long range surface plasmon polariton and dielectric waveguides," *Appl. Phys. Lett.*, vol. 90, pp. 241120-1–241120-3, 2007.
[23] F. Liu, R. Wan, Y. Rao, Y. Zheng, Y. Huang, W. Zhang, and J. Peng, "Hybrid three-arm coupler consisted of long range surface plasmon polariton and dielectric waveguides," *J. Lightw. Technol.*, vol. 26, no. 24, pp. 3872–3882, Dec. 2008.
[24] F. Liu, R. Wan, Y. Huang, and J. Peng, "Refractive index dependence of the coupling characteristics between long range surface plasmon polariton and dielectric waveguide mode," *Opt. Lett.*, vol. 34, pp. 2697–2699, 2009.
[25] R. Wan, F. Liu, X. Tang, Y. Huang, and J. Peng, "Vertical coupling between short range surface plasmon polariton mode and dielectric waveguide mode," *Appl. Phys. Lett.*, vol. 94, pp. 141104-1–141104-3, 2009.
[26] R. Wan, F. Liu, and Y. Huang, "Ultra-thin layer sensing based on hybrid coupler with short range surface plasmon polariton and dielectric waveguide," *Opt. Lett.*, vol. 35, pp. 244–246, 2010.
[27] A. Degiron, S. Y. Cho, T. Tyler, N. M. Jokerst, and D. R. Smith, "Directional coupling between dielectric and long-range plasmon waveguides," *New J. Phys.*, vol. 11, pp. 015002–015011, 2009.
[28] S. Y. Park, J. T. Kim, J. S. Shin, and S. Y. Shin, "Hybrid vertical directional coupling between a long range surface plasmon polariton waveguide and a dielectric waveguide," *Opt. Commun.*, vol. 282, pp. 4513–4517, 2009.
[29] F. Liu, R. Wan, Y. Li, Y. Huang, Y. Miura, D. Ohnishi, and J. Peng, "Extremely high efficient coupling between long range surface plasmon polariton and dielectric waveguide mode," *Appl. Phys. Lett.*, vol. 95, pp. 091104-1–091104-3, 2009.
[30] I. Breukelaar, R. Charbonneau, and P. Berini, "Long-range surface plasmon-polariton mode cutoff and radiation," *Appl. Phys. Lett.*, vol. 88, pp. 051119-1–051119-3, 2006.
[31] E. D. Palik, *Handbook of Optical Constants of Solids*. Orlando, FL: Academic, 1985, pp. 286–297.
[32] FEMLAB Electromagnetics Module Manual Ottawa-Carleton Inst. Elect. Comput. Eng., Sweden, 2003, 3.0 ed. COMSOL AB.
[33] I. G. Breukelaar, "Surface plasmon-polaritons in thin metal strips and slabs: Waveguiding and mode cutoff," Master Thesis, Ottawa Univ., , 2004, Chapter 4, p. 76.
[34] Q. Li and M. Qiu, "Structurally-tolerant vertical directional coupling between metal-insulator-metal plasmonic waveguide and silicon dielectric waveguide," *Opt. Exp.*, vol. 18, pp. 15531–15543, 2010.
[35] K. Okamoto, *Fundamentals of Optical Waveguides*. New York: Academic, 2000.
[36] W. P. Huang, "Coupled-mode theory for optical waveguides: An overview," *J. Opt. Soc. Amer. A*, vol. 11, no. 3, pp. 963–983, 1994.
[37] The $\beta_{\mathrm{SRSPP_r}}$ is far away from β_{SiN}, which leads to no influence when considering the coupling between LRSPP mode and SiN waveguide mode in this paper.

Fang Liu received the B.S. degree from the Beijing Institute of Technology, Beijing, China, in 2003, and the Ph.D. degree from the Department of Electrical Engineering, Tsinghua University, Beijing, China, in 2008.

He is currently an Assistant Professor at Tsinghua University. His current research interests include the area of integrated optical devices.

Yunxiang Li, biography not available at the time of publication.

Ruiyuan Wan, biography not available at the time of publication.

Yidong Huang received the B.S. and Ph.D. degrees in optoelectronics from Tsinghua University, Beijing, China, in 1988 and 1994, respectively.

From 1991 to 1993, she was with Arai Laboratories, Tokyo Institute of Technology, Tokyo, Japan, on leave from Tsinghua University. She was with the Photonic and Wireless Devices Research Laboratories, NEC Corporation, from 1994 to 2003, where she was engaged in the research on semiconductor laser diodes for optical-fiber communication. In 2003, she joined the Department of Electronics Engineering, Tsinghua University, as a Professor, where she is currently engaged in research on nanostructure optoelectronics.

Xue Feng, biography not available at the time of publication.

Wei Zhang, biography not available at the time of publication.